ELSEVIER

Journal of Alloys and Compounds 432 (2007) 96–102

Journal of ALLOYS AND COMPOUNDS

www.elsevier.com/locate/jallcom

Unexpected ordering behaviour of Pt_3Al intermetallic precipitates

A. Douglas [a,b,c], J.H. Neethling [b,c,*], R. Santamarta [d], D. Schryvers [d], L.A. Cornish [a,c]

[a] *Physical Metallurgy Division, Mintek, Private Bag X3015, Randburg 2125, South Africa*
[b] *Department of Physics, Nelson Mandela Metropolitan University, PO Box 77000, Port Elizabeth 6031, South Africa*
[c] *DST/NRF Centre of Excellence in Strong Materials, University of the Witwatersrand, Private Bag 3, Johannesburg 2050, South Africa*
[d] *Electron Microscopy for Material Sciences, University of Antwerp, Antwerp, Belgium*

Received 10 May 2006; received in revised form 25 May 2006; accepted 25 May 2006
Available online 12 July 2006

Abstract

Alloys with a microstructure analogous to the γ/γ′ system of Ni-based superalloys are found in the Pt–Al system. A two-phase microstructure consisting of Pt_3Al precipitates in an fcc (Pt) solid solution was developed to mimic the basic microstructure of Ni-based superalloys. The Pt_3Al precipitates were found to consist of plates that are twin related and have a specific orientation relationship with respect to the matrix. Each plate contains a high density of thin platelets lying perpendicular to the *c*-direction. The precipitates were expected to crystallise in the D0′*c* unit cell. However, the experimental results showed that a different ordered structure, based on two modifications of the D0′*c* unit cell, occurred instead. The observed matrix/precipitate orientation relationship could be justified by misfit considerations.

Keywords: Intermetallics; High temperature alloys; Crystal structure; Transmission electron microscopy (TEM)

1. Introduction

Ni-based superalloys are used in air and land-based turbines and owe their superior high temperature properties in part to their characteristic two-phase γ/γ′ microstructure. However, these alloys are used at the upper end of the operating temperature. The thermodynamic efficiency of an engine can be improved by increasing their operating temperature, but this requires alloys that are able to withstand such an increase. One approach is to design an alloy with a similar microstructure to the Ni-based superalloys, but then replace the Ni with an element with a higher melting point, such as Pt.

An analogous two-phase γ/γ′ structure forms in the Pt–Al system. The microstructure consists of a Pt solid solution matrix and Pt_3Al precipitates, which form by a eutectic reaction at a temperature of 1507 °C and with a eutectic composition of about 20 at.% Al [1]. The Pt_3Al precipitates have the cubic $L1_2$ structure at high temperature, but transform to a tetragonal distortion of this cubic structure upon cooling. This low temperature structure, which has been designated as D0′*c* [2], is closely related to that of Pt_3Ga [3]. Phases with tetragonally distorted structures have been reported in other alloy systems, including CuAuI in CuAu [4], Ni_3V [5] and the $Al_{11}Ti_5$ phase in $(Al,Ag)_3Ti$ [6].

In order to maintain the analogous γ/γ′ microstructure in the Pt–Al alloys over the whole operating temperature regime (room temperature to above 1100 °C), the $L1_2$ structure of the precipitates must be prevented from transforming to the tetragonal structure upon cooling. Some success has been achieved in stabilising the high temperature $L1_2$ form by ternary alloying of Pt and Al with Ti and Cr [7], as well as Sc [8]. However, the precipitates are distorted tetragonally in the simple binary Pt–Al alloy. This paper describes the microstructure and crystal structure of tetragonally distorted Pt_3Al precipitates in such a binary Pt–Al alloy.

2. Experimental

Arc-melted buttons were manufactured from pure elemental Pt and Al of at least 99.9% purity. The resulting binary alloy had a nominal composition of 86 at.% Pt and 14 at.% Al as determined by energy dispersive X-ray spectrometry (EDS) in a scanning electron microscope (SEM). The chosen composition lies within the two-phase field (Pt solid solution and Pt_3Al) of the Pt–Al constituency diagram. The alloy was heat treated for 96 h at 1350 °C, followed by furnace cooling. This heat treatment temperature was based on the target operating temperature for these alloys [7]. Cylinders with a diameter of 3 mm

* Corresponding author. Tel.: +27 41 5042143; fax: +27 41 5042573.
E-mail address: jan.neethling@nmmu.ac.za (J.H. Neethling).

0925-8388/$ – see front matter © 2006 Elsevier B.V. All rights reserved.
doi:10.1016/j.jallcom.2006.05.106

were cut from the buttons using spark erosion and were used to prepare TEM specimens.

The cylinders were sectioned into discs with a thickness of 1 mm, which were mechanically lapped to a thickness of 100 μm and dimpled to 30 μm. Low-angle (4°) argon ion milling was done at room temperature, and with an accelerating voltage of 4 kV, until foil perforation, using a Gatan PIPS™ ion mill. Compositional analysis was performed in a Philips XL30 SEM using the standardless analysis procedure of the EDAX DX4i energy dispersive X-ray spectrometry system. A Philips CM20 TEM operating at 200 kV was used for conventional transmission electron microscopy (CTEM) (including bright- and dark-field imaging and selected area diffraction (SAD)). High-resolution TEM was performed on a Jeol 4000EX HRTEM operated at 400 kV, in collaboration with Electron Microscopy for Materials Research (EMAT), University of Antwerp, Belgium. The atomic structure of the tetragonal (D0′c) phase of Pt_3Al was constructed by using the atomic positions determined by Bronger et al. [9] for the space group *P4/mbm*. The following Wyckoff positions were used: Al (4f), Pt (4e), Pt (4g), Pt (4h). Various unit cells were constructed in the JEMS (Stadelmann, P.A., CIME-EPFL, Lausanne, Switzerland, 2003) and Electron Diffraction (Morniroli, J.P., Université De Lille, France, 2003) software packages, which were also used to simulate the diffraction patterns. The unit cells were also constructed using MacTempas (Kilaas, R., MacTempas, Total Resolution, Berkeley, USA, 2003), and yielded the same results. MacTempas was also used to simulate the high-resolution TEM lattice images. The local diffraction conditions of small regions in the lattice images were obtained by Fourier transforms using the CRISP software (Calidris, Sollentuna, Sweden, 2001).

3. Results and discussion

3.1. Microstructure

A two-phase microstructure consisting of Pt_3Al precipitates in a (Pt) solid solution matrix was observed. The compositions of the Pt_3Al and (Pt) phases, as determined by standardless SEM EDS, are shown in Table 1.

The typical microstructure of the alloy is shown in the dark-field TEM micrograph, Fig. 1(a). The precipitates appear bright and the matrix dark since a chemically sensitive reflection ($1\,\bar{1}\,0$ in Fig. 2a) from the precipitates was used to form the image. The Pt_3Al precipitates had a trimodal size distribution, with primary precipitates larger than 2 μm (not shown), secondary precipitates approximately 1 μm in diameter, and a high volume fraction of cube-shaped tertiary precipitates with a diameter of less than 50 nm.

A bright-field micrograph of the morphology of a typical secondary precipitate is shown in detail in Fig. 1(b). This precipitate consists of a number of stacked plates with thickness 200–400 nm. Two adjacent plates are designated (1) and (2) in Fig. 1(b). This kind of microstructure is similar to that observed for precipitates in other materials where an fcc-to-tetragonal distortion had taken place, such as Ni_3V [5] and $D0_{23}Al_{11}Ti_5$ [6]. The stacked plates in the Pt_3Al precipitates exhibit sets of narrow parallel lines, or platelets, perpendicular to the [0 0 1] directions in the stacked plates.

Table 1
Composition of matrix and precipitate phase (at.%)

Element	Matrix: (Pt) phase (at.%)	Precipitate: Pt_3Al phase (at.%)
Al	13 ± 2	27 ± 2
Pt	87 ± 2	73 ± 2

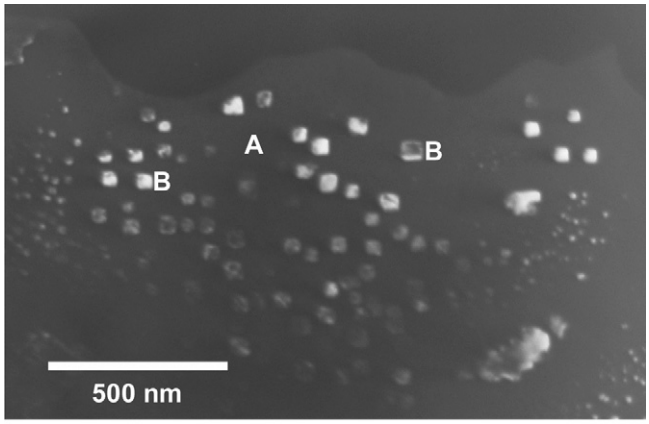

(a)

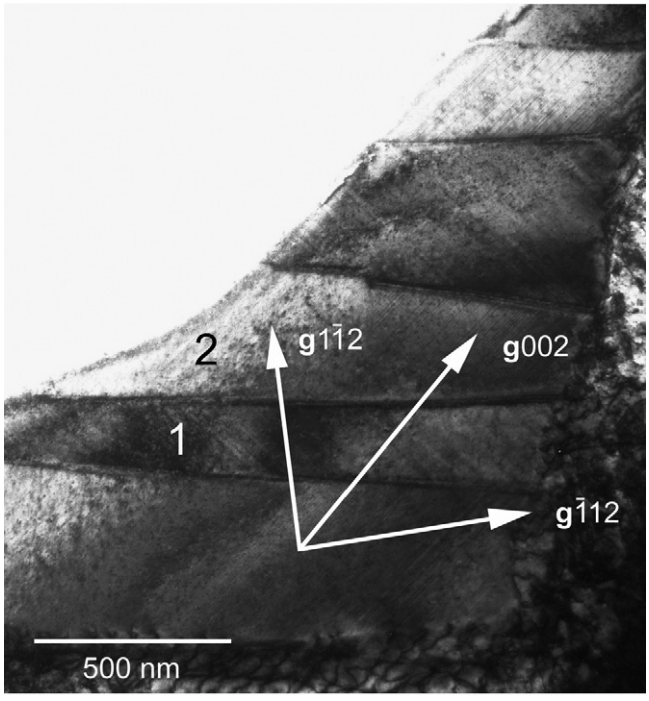

(b)

Fig. 1. (a) Dark-field TEM micrograph showing γ′ precipitates (bright) embedded in the matrix (dark). The $1\,\bar{1}\,0$ reflection in Fig. 2(a) was used to form the image. (b) Bright-field TEM micrograph of a γ′ precipitate containing stacked plates (e.g. 1 and 2); **g** vectors are labelled relative to the precipitate diffraction pattern.

3.2. Analysis of diffraction patterns

Selected area diffraction patterns for the matrix and the precipitate are shown in Fig. 2(a) and (b), respectively. The selected area aperture was positioned to include two adjacent plates in the precipitate. The SAD pattern of the matrix was simulated along the [0 0 1] beam direction based on an fcc unit cell. This simulation is shown in Fig. 2(c). The SAD pattern of the precipitate was simulated along the [1 1 0] beam direction, based on the D0′c (Pt_3Ga) unit cell, and is shown in Fig. 2(d). The size of the spots in the simulated diffraction patterns indicates the relative kinematical intensity of the reflections.

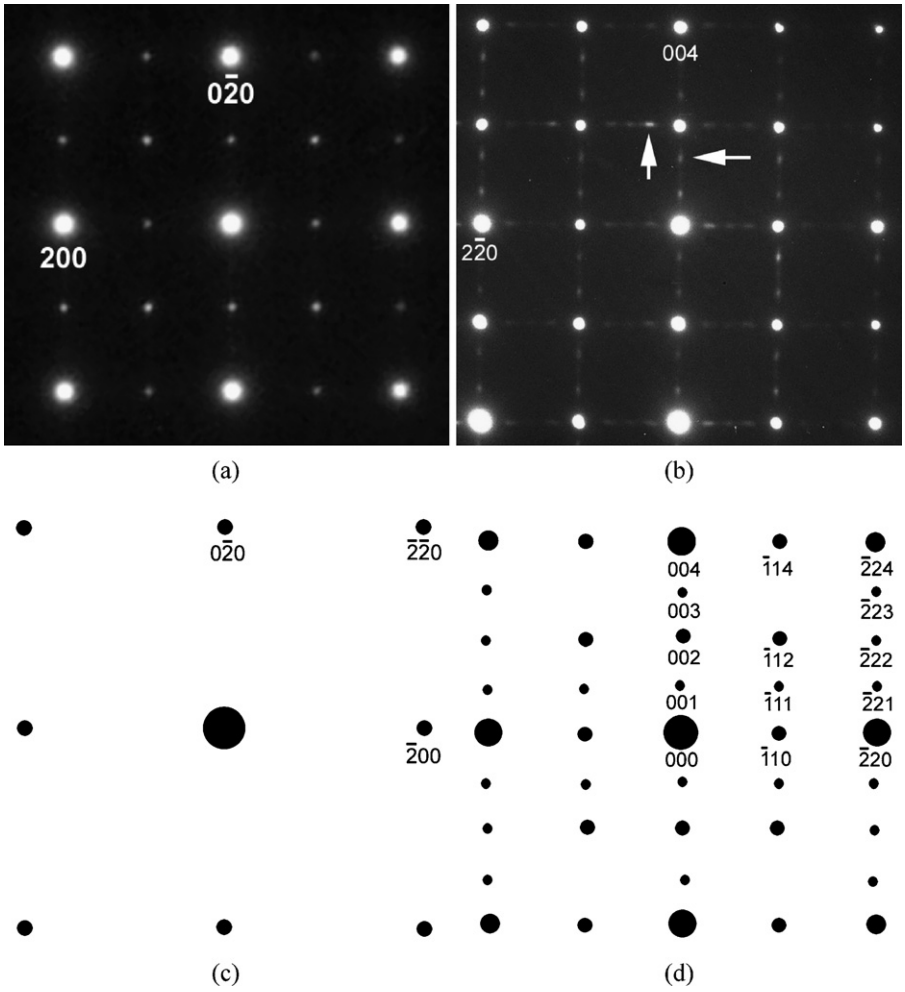

Fig. 2. (a) SAD pattern corresponding to the matrix, **B** = [0 0 1]. (b) SAD pattern corresponding to the precipitate, **B** = [1 1 0]. (c) Simulated matrix SAD pattern, **B** = [0 0 1]. (d) Simulated precipitate SAD pattern, **B** = [1 1 0].

The matrix diffraction pattern, which is supposed to be from a disordered fcc phase, contains faint extra spots in addition to the fundamental reflections expected for the fcc structure. There is a high density of small precipitates throughout the matrix, which makes it impossible to isolate the information contributed to the diffraction pattern by the matrix by using the selected area aperture. The matrix diffraction pattern is thus a composite of the diffraction patterns from the matrix and the precipitates.

The experimental γ' precipitate diffraction pattern contains fine structure in the form of additional extra spots (indicated by an arrow, Fig. 2(b)) that are found neither in the experimental matrix nor in the simulated D0′*c* diffraction pattern. The primary spots in the experimental SAD pattern of the γ' phase (Fig. 2(b)), e.g. 2 $\bar{2}$ 0, 2 $\bar{2}$ 4 and 0 0 4, match the high intensity reflections of the simulated diffraction pattern that is based on the D0′*c* structure (Fig. 2(d)). However, the following differences exist in the fine structure of the precipitate SAD pattern:

- The experimental pattern does not contain the ±0 0 1 and 0 0 3 reflections, which are allowed reflections for the D0′*c* structure.
- The experimental SAD pattern, Fig. 2(b), contains extra spots with reciprocal lattice vectors ±1/3[0 0 2] and ±2/3[0 0 2].

The platelets in the secondary precipitate are shown in greater detail in Fig. 3. They appear dark in bright-field (Fig. 3(a)), and bright in dark-field (Fig. 3(b)), and are associated with the extra spots in the diffraction pattern. Fig. 3(b) was obtained by using the reflections 1/3[0 0 2] and 2/3[0 0 2] in Fig. 2(a).

The existence of the extra spots suggests that some form of ordering exists within the platelets. It is likely that the platelets have a different structure factor and extinction distance compared to the adjacent regions, since the fine platelets appear dark in the bright-field image. The fine structure in the simulations of the Pt_3Al SAD patterns, using the D0′*c* unit cell, did not match the experimental results. As a result, various modified D0′*c* unit cells were investigated, and the observed features could be explained with two of these modified unit cells.

3.3. The modified D0′*c* unit cell

The atomic configuration of the D0′*c* structure, projected along the [1 1 0] direction, is shown in Fig. 4(a). The simu-

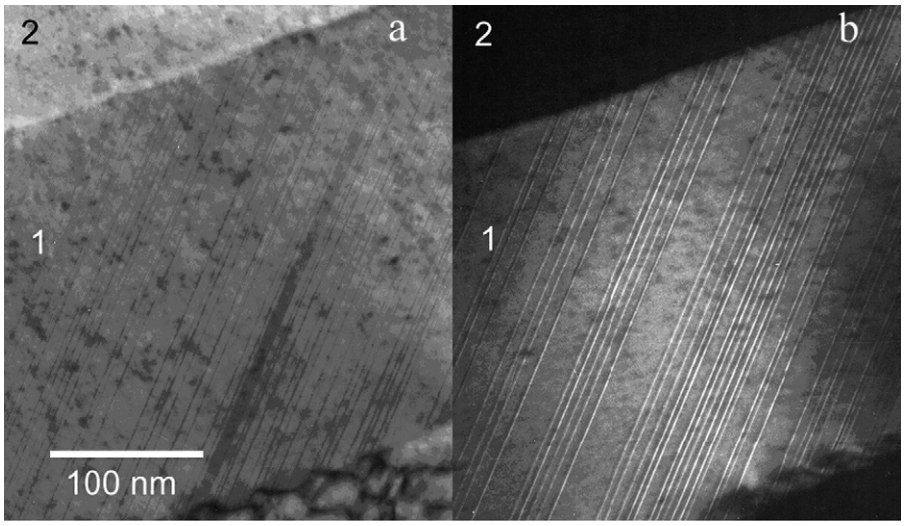

Fig. 3. (a) Bright-field image of platelets in plate 1 in Fig. 1(a). (b) Dark-field image of platelets in plate 1 in Fig. 1(a).

lated diffraction pattern using this unit cell is the one shown in Fig. 2(d). A modified tetragonal Pt_3Al unit cell, with the *c*-axis equal to 1.5 times that of the D0′*c* structure, was assumed to be the true structure of the Pt_3Al phase as shown in Fig. 4(b). The modified unit cell was constructed by repeating the top half of the D0′*c* structure, as shown in the dashed rectangles in Fig. 4. The simulated SAD pattern, based on the modified unit cell, is shown in Fig. 4(c). A selected area diffraction pattern of a single broad precipitate plate is shown in Fig. 4(d). The simulated SAD pattern based on the modified D0′*c* unit cell clearly agrees well with the experimental diffraction pattern. The atomic structure was investigated in more detail using HRTEM.

An experimental HRTEM micrograph of the boundary between two broad plates is shown in Fig. 5. The twinned nature of the two plates is clearly observed from the dark lines that lie perpendicular to each other across the plate boundary. Fourier transforms of three different small areas in Fig. 5 that give the local diffraction conditions, confirm this twinning. In plate 1, the extra superlattice reflections lie along the *c*-direction (perpendicular to the dark lines, inset a), both sets of extra spots are observed in the boundary (inset b) while the extra spots in plate 2 lie along the *c*-direction perpendicular to the dark lines in this plate (inset c). The fact that the extra spots lie perpendicular to one another proves that plates 1 and 2 are twinned.

Fig. 5 shows that the plates have two different types of atomic arrangement. For example, the region enclosed in the black circle consists of a number of rows of atomic columns that all have the same intensity. This contrasts with the region in the white circle where there is a periodic arrangement of bright atomic rows separated by a less intense row. This phenomenon can also be explained by the modified D0′*c* unit cell.

A HRTEM lattice image of a region of a Pt_3Al plate that exhibits double rows of bright spots (perpendicular to the *c*-axis) separated by a dark band is shown in Fig. 6. The matched simulated HRTEM image based on the modified D0′*c* unit cell is overlaid (top) on Fig. 6. The double bright rows correspond to planes in the unit cell that contain only platinum. These bright spots also correspond to atomic columns where platinum atoms that lie above one another are shifted laterally with respect to each other. The less intense rows are those where the Pt atoms lie almost on top of each other. The Fourier transform of this region is also overlaid (bottom). The extra spots due to the ordering can clearly be seen in this Fourier transform.

An enlargement of an area of the lattice image of a Pt_3Al precipitate, where all the atomic columns are bright, is shown in Fig. 7(a). A Fourier transform of this region is inset (bottom) in Fig. 7(a). The Fourier transform contains only the fundamental reflections, with no extra reflections that are due to the modified unit cell. This result can be explained if the precipitates are assumed to contain a second modification of the D0′*c* unit cell which consists of a unit cell that is half that of the D0′*c* unit cell in the *c*-direction. This second modified unit cell is shown in Fig. 7(b). A simulated HRTEM image based on this second unit cell modification matches the experimental image exactly and is inset (top) in Fig. 7(a).

Völkl et al. [8] used the Pt_3Ga structure type in their analysis of X-ray diffraction spectra of γ' precipitates (with a phase designated $Pt_{85}Al_{15}$ which they call $Pt_3Al(r)$ but which corresponds to D0′*c* in this work) in the Pt–Al–Sc system, but they did not observe the additional ordering that was observed here in the electron diffraction patterns.

4. Discussion

Phase transformations, in general, are accompanied by crystal lattice rearrangements [10]. The macroscopic shape of regions of a new phase within the parent phase is determined by the homogeneous strain of the transformation. The new phase crystals will generally have a different orientation from that of the parent phase due to the parent phase symmetry [10]. In the case of a cubic-to-tetragonal transformation, the resulting tetragonal crystals can have three different possible orientations relative to the parent phase. The tetragonal axis (*c* or [0 0 1]) may lie along any of the cube axes of the parent phase, i.e. the [1 0 0] (or *a* axis), [0 1 0] (or *b* axis) or [0 0 1] (or *c* axis) directions [11]. The difference in the crystal lattices of the parent phase and the

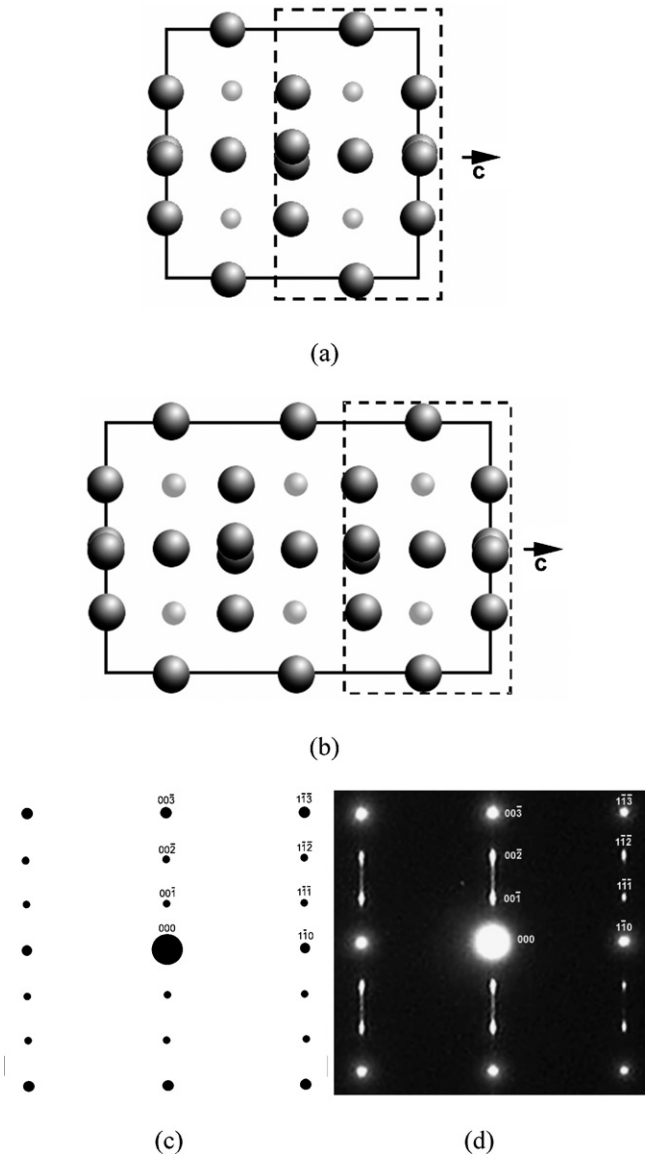

Fig. 4. (a) Unit cell of the D0′c structure, **B** = [1 1 0]. (b) Unit cell of modified D0′c unit cell, **B** = [1 1 0]. (c) Kinematically simulated SAD pattern of modified D0′c unit cell, **B** = [1 1 0]. (d) Experimental SAD pattern from a single broad plate, **B** = [1 1 0].

new phase requires atomic displacements in order for the two phases to fit together such that the elastic strain between the two phases are minimised. A characteristic morphology exists for the daughter phase precipitates due to these displacements.

Precipitates of tetragonal $D0_{23}Al_{11}Pt_5$ in an $L1_2(Al,Ag)_3Ti$ matrix were shown to consist of a thin-plate, multi-domain structure [6]. This multi-domain structure consisted of two types of twin, with the tetragonal axis of twin I parallel to the [1 0 0] matrix direction and the tetragonal axis of twin II parallel to the [0 1 0] matrix direction. The following orientation relationships were described [6]:

$$(1\,0\,0)I_P||(0\,0\,1)_M \quad \text{and} \quad \text{near } [0\,0\,1]I_P||[1\,0\,0]_M \tag{1}$$

$$(1\,0\,0)II_P||(0\,0\,1)_M \quad \text{and} \quad \text{near } [0\,0\,1]II_P||[0\,1\,0]_M \tag{2}$$

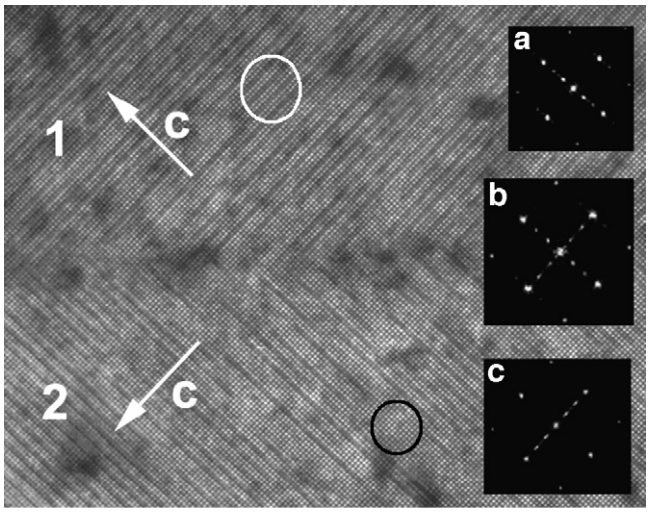

Fig. 5. Experimental HRTEM image of a twin boundary between two precipitate plates. (a) Fourier transform of plate 1. (b) Fourier transform of the twin boundary. (c) Fourier transform of plate 2.

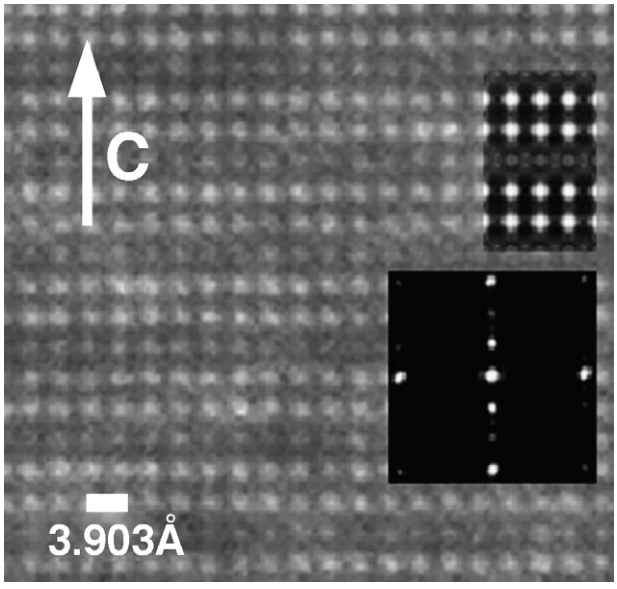

Fig. 6. Experimental HRTEM lattice image of a region of a Pt_3Al plate containing double rows of bright atomic columns separated by a dark row. The matched simulated HRTEM image (top) and Fourier transform (bottom) are inset.

The misfit between the Pt_3Al and (Pt) phase can be calculated by considering equivalent parameters. The lattice parameters for the (Pt) (cubic) and Pt_3Al (tetragonal) phases of the Pt_{75}:Al_{25} alloy are given in Table 2. The (0 0 1) projection of the unit cells of the (Pt) and Pt_3Al phases, is shown in Fig. 8.

Table 2
Experimentally determined lattice parameters for cubic and tetragonal phases in a binary Pt–Al alloy

	(Pt) phase, cubic (Å)	Pt_3Al phase (tetragonal) (Å)
a and b	3.92 ± 0.06	5.45 ± 0.06
c	–	7.82 ± 0.06

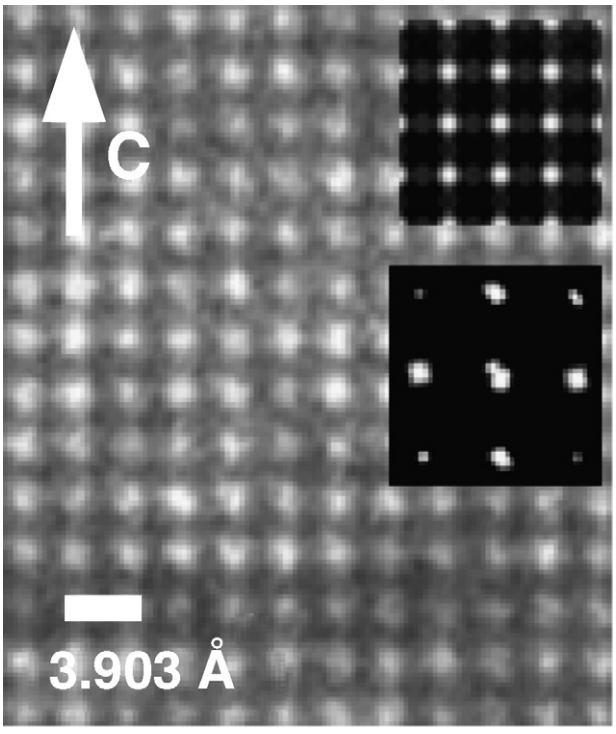

Fig. 7. (a) Experimental HRTEM lattice image of a region of a Pt_3Al plate, where all atomic columns are bright. The matched simulated HRTEM image (top) and Fourier transform (bottom) are inset. (b) Schematic illustration of the second modified D0′c unit cell (Pt: dark; Al: light).

Table 3
Misfit between cube directions in cubic and tetragonal phases

Direction	Misfit (%)
$[1\,0\,0]_{M,P}$	39.1
$[0\,1\,0]_{M,P}$	39.1
$[0\,0\,1]_{M,P}$	99.3

The misfit, δ, between the cubic and tetragonal axes along the directions implied in the orientation relationships (1) and (2) above, are given in Table 3. These values were calculated using the expression:

$$\delta = \frac{a_P - a_M}{a_M} \times 100\% \tag{3}$$

where a_P is the lattice parameter of the precipitate and a_M that of the matrix.

If the orientation relationships as described in (1) and (2) above are applied to the Pt_3Al alloy, a large misfit, with a correspondingly high misfit strain, would result. An orientation relationship that minimises the misfit in the Pt–Al alloy should exist.

Consider an orientation relationship where the c-axis of the tetragonal unit cell is still aligned along the c-axis of the cubic unit cell, but such that the tetragonal cell is rotated by 45° about its c-axis. Then, in general, the following orientation relationship holds:

$$(1\,1\,0)_P||(0\,0\,1)_M, \qquad (0\,0\,1)_P||(1\,0\,0)_M \quad \text{and}$$
$$[0\,0\,1]_P||[1\,0\,0]_M \tag{4}$$

The length a', parallel to the $[1\,1\,0]_P$ direction, is equal to 3.860 Å. Also note that, for the cubic phase, $2c = 7.848$ Å, which is only slightly greater than the value of 7.819 Å for c of the tetragonal phase, implying a small misfit along the $\langle 1\,0\,0\rangle$ and $[0\,0\,1]$ matrix and precipitate directions, respectively. The misfits along the given directions in the matrix and precipitate, as determined from Eq. (3), are shown in Table 4. Precipitates with the orientation relationship described in (4) above with respect

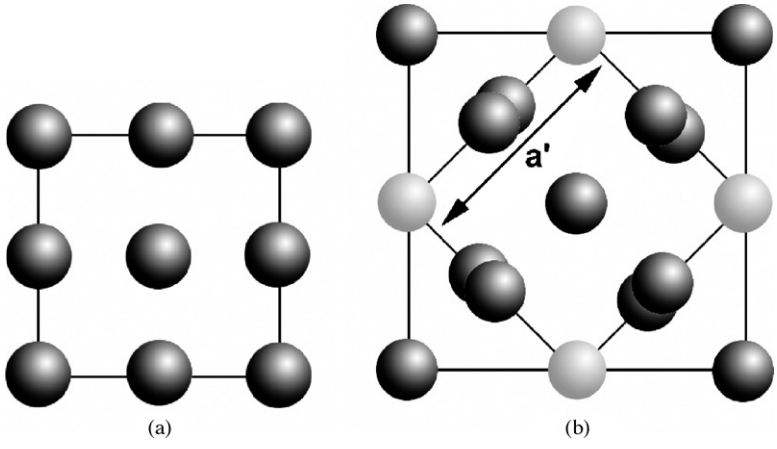

Fig. 8. (a) (0 0 1) projection of the fcc unit cell of the (Pt) phase. (b) (0 0 1) projection of the modified D0′c unit cell of the Pt_3Al phase.

Table 4
Misfit along equivalent directions using the orientation relationship in (4)

Direction	Misfit (%)
$[0\,1\,0]_M$; $[\bar{1}10]_P$	−1.6
$[1\,0\,0]_M$; $[1\,1\,0]_P$	−1.6
$2c[0\,0\,1]_M$; $[0\,0\,1]_P$	−0.4

to the matrix will, therefore, have a smaller misfit with the matrix.

The results of this investigation indicates that the structure of the Pt_3Al can be described by two modifications of the D0′c structure, one with half the c-constant and the other with 1.5 the c-constant. Various combinations of integer multiples of these two cells will have approximately the same misfit with respect to the matrix as the D0′c structure. For example, $1/2c + 1.5c = 2c \approx 4a$, or $1/2c + 1/2c = c \approx 2a$. The (0 0 1) projections of the two modified D0′c unit cells are identical to that of the unmodified cell, which means that the orientation relationship derived for the D0′c unit cell from the misfit considerations above can be applied to the modified cases without loss of generality.

The Pt_3Al precipitates consist of a multi-domain structure in the form of parallel plates. One of the Pt_3Al plates, say plate 1, can be considered to consist of tetragonally distorted Pt_3Al such that the c-axis of the tetragonal unit cell is aligned along the c-axis of the cubic cell, i.e.:

$$[0\,0\,1]_P||[1\,0\,0]_M, \quad (0\,0\,1)_P||(1\,0\,0)_M \quad \text{and} \quad (1\,1\,0)_P||(0\,1\,0)_M \tag{5}$$

In plate 2, the c-axis of the tetragonal Pt_3Al lies along the b-axis of the cubic unit cell such that the following orientation relationships hold:

$$[0\,0\,1]_P||[0\,1\,0]_M, \quad (0\,0\,1)_P||(0\,1\,0)_M \quad \text{and} \quad (1\,1\,0)_P||(0\,0\,1)_M \tag{6}$$

These two plates are twinned with respect to one another, with the twin plane being the $\{1\,1\,3\}$ plane for the modified unit cell.

5. Conclusions

The Pt_3Al precipitates in a Pt–Al analogue of Ni-based superalloys had a trimodal size distribution, ranging from less than 50 nm to greater than 1 μm. The larger precipitates were found to consist of stacked plates that are twin related, and each twin plate contains a high density of thin platelets lying perpendicular to the c-direction. Electron diffraction experiments showed an unexpected result in the form of extra spots in the diffraction pattern. These extra spots as well as the appearance of HRTEM lattice images could be fully explained by two modifications of the D0′c unit cell: one that was 1.5 times the length of the c-axis of this unit cell, and one that was 1/2 the length of the unit cell. The c-axis of the unit cell of the precipitate was aligned along the a- and b-axes of the matrix unit cell. This matrix/precipitate orientation relationship formed in order to relieve the lattice misfit.

Acknowledgements

The authors would like to thank Mintek, the South African Department of Science and Technology (DST), the Platinum Development Initiative (PDI) and the National Research Foundation (NRF) for financial support.

References

[1] A.J. McAlister, D.J. Kahan, Bull. Alloy Phase Diagrams 7 (1986) 47.
[2] Y. Mishima, Y. Oya, T. Suzuki, Proceedings of the International Conference on Martensitic Transformations, Japan Institute of Metals, 1986, p. 1009.
[3] T. Chattopadhay, K. Schubert, J. Less-Common Met. 41 (1975) 19.
[4] M. Hirabayashi, S. Weissmann, Acta Metall. 10 (1962) 25.
[5] L.E. Tanner, Phys. Status Solid 30 (1968) 685.
[6] W.H. Tian, M. Nemoto, Mater. Sci. Eng. A329–331 (2002) 653.
[7] P.J. Hill, T. Biggs, P. Ellis, J. Hohls, S.S. Taylor, I.M. Wolff, Mater. Sci. Eng. A301 (2001) 167.
[8] R. Völkl, Y. Yamabe-Mitarai, C. Huang, H. Harada, Metall. Mater. Trans. A 36a (2005) 2881.
[9] W. Bronger, K. Wrzesien, P. Müller, Solid State Ionics 101–103 (1997) 633.
[10] A.G. Khachaturyan, Theory of Structural Transformations in Solids, John Wiley and Sons, New York, 1983.
[11] V.I. Syutkina, E.S. Yakovleva, Phys. Status Solidi 21 (1967) 465.